

Equation of State of Liquid Iron under Extreme Conditions

Yasuhiro Kuwayama^{1,2,*} Guillaume Morard^{3,4} Yoichi Nakajima^{5,6,†} Kei Hirose^{1,7,‡} Alfred Q. R. Baron⁶,
Saori I. Kawaguchi⁸ Taku Tsuchiya² Daisuke Ishikawa^{6,8} Naohisa Hirao⁸ and Yasuo Ohishi⁸

¹Department of Earth and Planetary Science, The University of Tokyo, 113-0033 Tokyo, Japan

²Geodynamics Research Center, Ehime University, 790-8577 Ehime, Japan

³Sorbonne Université, Institut de Minéralogie, de Physique des Matériaux et de Cosmochimie, IMPMC,
Museum National d'Histoire Naturelle, UMR CNRS, 7590 Paris, France

⁴Université Grenoble Alpes, Université Savoie Mont Blanc, CNRS, IRD, IFSTTAR, ISTERre, 38000 Grenoble, France

⁵Department of Physics, Kumamoto University, 860-8555 Kumamoto, Japan

⁶Materials Dynamics Laboratory, RIKEN SPring-8 Center, 679-5148 Hyogo, Japan

⁷Earth-Life Science Institute, Tokyo Institute of Technology, 152-8550 Tokyo, Japan

⁸SPring-8, Japan Synchrotron Radiation Research Institute, 679-5198 Hyogo, Japan



(Received 6 August 2019; accepted 10 March 2020; published 22 April 2020)

The density of liquid iron has been determined up to 116 GPa and 4350 K via static compression experiments following an innovative analysis of diffuse scattering from liquid. The longitudinal sound velocity was also obtained to 45 GPa and 2700 K based on inelastic x-ray scattering measurements. Combining these results with previous shock-wave data, we determine a thermal equation of state for liquid iron. It indicates that Earth's outer core exhibits 7.5%–7.6% density deficit, 3.7%–4.4% velocity excess, and an almost identical adiabatic bulk modulus, with respect to liquid iron.

DOI: 10.1103/PhysRevLett.124.165701

Iron is the sixth most abundant element in the universe and the main component of dense metallic cores of planets. This is not only true for Earth, but also for Mercury and Mars, which are expected to have partially molten cores [1,2]. Density (ρ) and longitudinal sound velocity (V_p) (equivalent to bulk sound velocity, V_Φ , in a liquid) are the primary observables of Earth's liquid outer core [3]. Therefore, laboratory measurements of these properties at high pressure are of great importance to understand Earth's and other planets' core composition and behavior.

While determination of density for crystalline materials under high pressure and temperature (P - T) is relatively straightforward by *in situ* x-ray diffraction (XRD), it is still challenging for disordered materials. Although XRD is potentially applied up to 100 GPa and high temperature, analytical methods to extract ρ from a diffuse XRD signal, which is characteristic of a liquid, are not yet well established; a recent study [4] concluded that a conventional technique to analyze the diffuse signals gives a liquid density with uncertainty exceeding more than 10%. Improvement of the diffuse scattering analysis is therefore necessary. In particular, the density of liquid iron has not been reported at high pressure based on static experiments.

V_p is also a key property to understand liquid behavior as it is related to compressibility, thermal expansivity, the Grüneisen parameter (γ), etc. In particular, it is an important quantity for constructing an equation of state (EOS) of a liquid when combined with density data. Previously, the V_p of liquid iron was obtained only to 5.8 GPa by ultrasonic

measurements in a multi-anvil apparatus [5]. This is much lower than the pressure range of the Earth's core. Moreover, the structure of liquid iron may be different above 6 GPa [6], indicating that measurements are needed to higher pressures to understand the core.

In this study, we measured the density of liquid iron at pressures up to 116 GPa and 4350 K via static compression using a laser-heated diamond-anvil cell (LH-DAC). This is close to conditions at the top of Earth's core. A new analytical method was applied to derive ρ from diffuse x-ray scattering signals, as this is key to precise determination of liquid density under pressure. We also obtained the V_p of liquid iron to 45 GPa by inelastic x-ray scattering (IXS) measurements in the LH-DAC. From our new data combined with previous shock-wave data [7,8], we obtain the P - T - ρ - V_p - γ relation for Earth's entire outer core conditions (136–330 GPa, 4000–5400 K) based on the Mie-Grüneisen EOS. The earlier shock compression experiments measured the ρ , V_p , and γ of liquid iron only between 278 and 397 GPa along the Hugoniot path that intersects the melting curve of iron around 270 GPa [7]. The temperature in shock experiments is not well determined, being dependent on the model of internal energy of liquid iron. We therefore do not employ the temperature data reported in the shock experiments.

We collected angle-dispersive XRD spectra using a brilliant x-ray beam at BL10XU, SPring-8 [9] (see Supplemental Material [10], Sec. I). Strong diffuse scattering signals from molten iron were found in the XRD

spectra collected at about 100–400 K above its melting point (Fig. S1 in Ref. [10]). A background is subtracted (based on the measurement just below the melting point), and the result is converted into the structure factor $S(Q)$, where Q is the momentum transfer. Transformation of $S(Q)$ gives the distribution function $F(r)$ and the radial distribution function $g(r)$ (r , radial distance) [Fig. 1] (Eqs. S6 and S7 in Ref. [10]).

The density of the liquid, in principle, can be determined from the slope of $F(r)$ for r smaller than the interatomic spacing, where $F(r) = -4\pi\rho r$ and $g(r) = 0$. However, the transformation from Q to r requires integration over $Q \rightarrow$ infinity. Experimental limits on the Q range result

in oscillations in $F(r)$ and $g(r)$ that lead to large uncertainty in the determination of density if not corrected. An iterative analytical procedure originally developed in Ref. [25] has been applied for liquid density determinations at high pressure [26,27], but it often fails [4]. Indeed, it modifies $S(Q)$ from the experimentally observed one, losing information from raw data.

In this study, we have developed an innovative analytical method in which the observed $S(Q)$ is extended beyond Q_{\max} (the maximum Q in experimental data) so that the corresponding $g(r)$ is physically reasonable; $g(r) = 0$ for $r < r_{\min}$ region (r_{\min} , the distance between the nearest-neighboring atoms). We extend $S(Q)$ by

$$S_{\text{extend}}(Q) = \begin{cases} S(Q) & (Q \leq Q_{\max}) \\ 1 - \frac{1}{Q} \int_0^{r_{\min}} \{4\pi r \rho + \frac{2}{\pi} \int_0^{Q_{\max}} f(Q) \sin(Qr) dQ\} \sin(Qr) dr & (Q > Q_{\max}) \end{cases}, \quad (1)$$

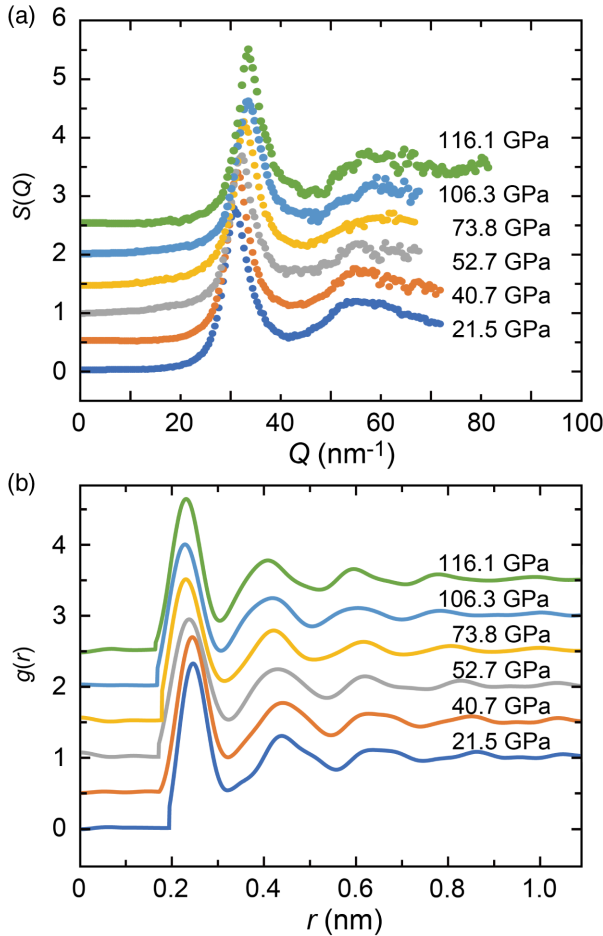


FIG. 1. Structural analyses of liquid iron at high pressures via *in situ* XRD measurements. (a) Structure factor $S(Q)$ of liquid iron up to 116.1 GPa determined from XRD measurements in this study, showing peak shifts to larger Q values due to the compression of liquid iron. (b) Corresponding radial distribution functions, $g(r)$, determined in this study. Vertical scales are offset for clarity for both $S(Q)$ and $g(r)$ plots.

where $f(Q) = Q\{S(Q) - 1\}$ (see Supplemental Material [10], Sec. II). The transformed quantities $F_{\text{extend}}(r)$ and $g_{\text{extend}}(r)$ are calculated from the $S_{\text{extend}}(Q)$. However, there are several unknowns in the procedure, including a scale factor for background s , normalization of $S(Q)$, α_N , as well as desired ρ and r_{\min} . If incorrect values are used for them, the difference between calculated $F_{\text{extend}}(r)$ and expected $F(r) = -4\pi\rho r$ [or between calculated $g_{\text{extend}}(r)$ and expected $g(r) = 0$] at $r < r_{\min}$ will be larger compared to that calculated for true values. For instance, if input ρ includes error $\Delta\rho$ as $\rho_{\text{input}} = \rho_{\text{true}} + \Delta\rho$, $F_{\text{extend}}(r)$ calculated from $S_{\text{extend}}(Q)$ involves an additional term given by

$$\frac{2}{\pi} \int_{Q_{\max}}^{\infty} \left\{ \int_0^{r_{\min}} -4\pi r \Delta\rho \sin(Qr) dr \right\} \sin(Qr) dQ, \quad (2)$$

(see Supplemental Material [10]). We sought the best $S_{\text{extend}}(Q)$, as well as s , α_N , ρ , and r_{\min} , by minimizing χ^2 (see Ref. [25]) given by

$$\chi^2(s, \alpha_N, \rho, r_{\min}) \equiv \int_0^{r_{\min}} \{g_{\text{extend}}(r)\}^2 dr. \quad (3)$$

We searched for the minimum χ^2 in wide ranges of s , α_N , ρ , and r_{\min} ; 1 ± 0.5 for s (s is expected to be within 1 ± 0.05 , since the fluctuation in incident x-ray intensity was less than 5%), $\pm 50\%$ from the value obtained by the Krogh-Moe and Norman's method [28,29] for α_N , $\pm 50\%$ from the density of solid iron at the P - T condition of an experiment for ρ , and between 0.15 and 0.30 nm for r_{\min} [0.30 nm is larger than the first peak position in $g(r)$]. For $r_{\min} < 0.15$ nm, a small subpeak appeared between $r = 0.15$ nm and the dominant peak in $g(r)$. The existence of such a subpeak is unreasonable, because liquid iron is expected to be a simple monoatomic liquid.

TABLE 1. Experimental results on liquid iron.

$P - T - \rho$ relation determined from XRD measurements			
Run No.	P (GPa) ^a	T (K) ^b	ρ (g/cm ³) ^a
No. 1	21.5(12)	2600	7.91(7)
No. 2	31.3(17)	2870	8.24(11)
No. 3	40.6(5)	2880	8.64(15)
No. 4	40.7(21)	3060	8.48(9)
No. 5	52.7(16)	3250	8.93(7)
No. 6	52.8(18)	3340	9.19(13)
No. 7	68.5(22)	3530	9.32(10)
No. 8	69.8(19)	3540	9.30(11)
No. 9	73.8(24)	3630	9.53(7)
No. 10	106.3(35)	4250	10.01(11)
No. 11	116.1(39)	4350	10.10(14)
$P - T - V_P$ relation determined from IXS measurements			
Run No.	P (GPa) ^a	T (K) ^b	V_P (km/s) ^a
No. 12	16.0(16)	2200	5.03(12)
No. 13	32.7(11)	2700	5.40(32)
No. 14	44.9(20)	2700	5.82(20)

^aThe numbers in parentheses represent 1 standard deviation in the last digits.

^b $\pm 10\%$ uncertainty [10].

In practice, the shape of artificial oscillations in $F_{\text{extend}}(r)$ and $g_{\text{extend}}(r)$ are also affected by Q_{max} in Eq. (1) [30,31]. Therefore, we calculated χ^2 with changing Q_{max} from the experimental limit to $\sim 30 \text{ nm}^{-1}$ that corresponds to the position at the end of the first dominant peak in $S(Q)$. The calculation shows that there is a unique Q_{max} at $\sim 70 \text{ nm}^{-1}$ which minimizes χ^2 for each experimental data. When Q_{max} is smaller than 65 nm^{-1} , the calculated χ^2 is larger than the minimum χ^2 by more than 2 orders of magnitude. For run No. 1 (Table I), for example, we find a unique set of these parameters that minimizes χ^2 ;

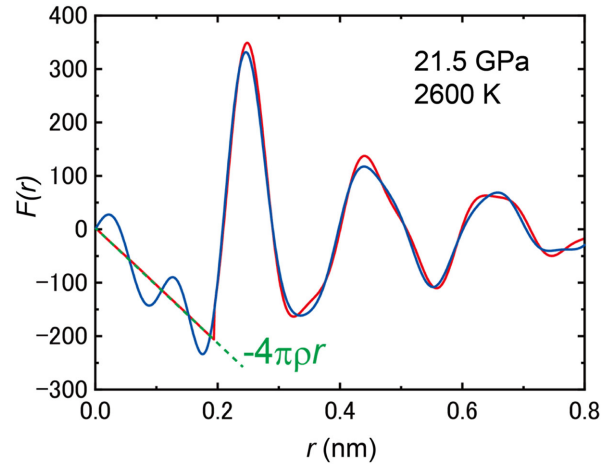


FIG. 2. Distribution function $F(r)$ from run No. 1 calculated based on the present analytical method (red), in which the extension of $S(Q)$ and parameters of s , α_N , and ρ are determined simultaneously, demonstrating that our new method successfully reduces the oscillations at $r < r_{\text{min}}$ and gives a precise liquid density from the slope. $F(r)$ calculated without extension of $S(Q)$ with assuming $s = 1$ is shown by the blue line for comparison.

$s = 1.0052$, $\alpha_N = 4.522$, $r_{\text{min}} = 0.194 \text{ nm}$, and $Q_{\text{max}} = 72.0 \text{ nm}^{-1}$, giving $\rho = 85.26 \text{ atoms/nm}^3$ (7.91 g/cm^3) (Fig. S9 in the Supplemental Material [10]). Figure 2 shows $F_{\text{extend}}(r)$ and $g_{\text{extend}}(r)$ calculated from $S_{\text{extend}}(Q)$ for run #1, indicating that our procedure successfully reduced the oscillations in $F(r)$ and $g(r)$ at $r < r_{\text{min}}$ that are mainly caused by a lack of data beyond experimental Q and inaccurate s and α_N . The uncertainty in ρ estimated from the difference between calculated $F_{\text{extend}}(r)$ and expected $F(r) = -4\pi\rho r$ is found to be less than $\sim 1\%$ (Table I). Note that our procedure does not modify $S(Q)$ at $Q \leq Q_{\text{max}}$, in contrast to previous iterative analytical procedures.

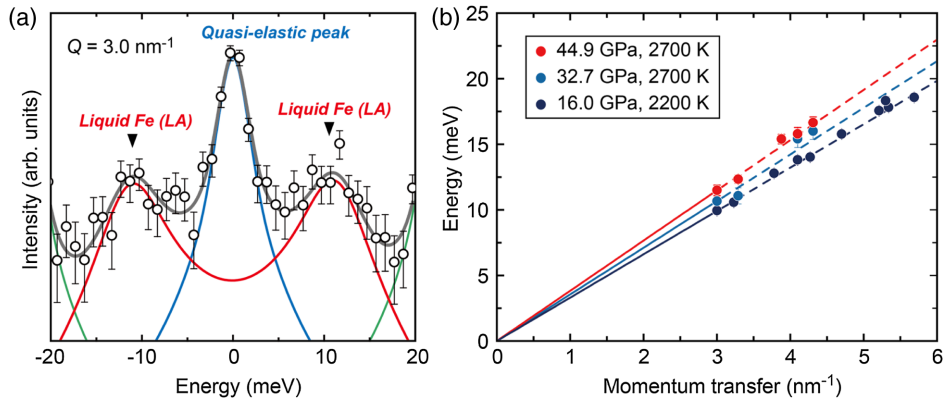


FIG. 3. High-pressure inelastic x-ray scattering (IXS) measurements of liquid iron. (a) Typical IXS spectrum of liquid iron collected at 44.9 GPa and 2700 K at momentum transfer $Q = 3.0 \text{ nm}^{-1}$. The spectra include three components: a quasielastic peak near zero energy transfer (blue), longitudinal acoustic (LA) phonon mode of liquid Fe (red), and transverse acoustic (TA) phonon mode of diamond (green). The vertical axis is plotted on a logarithmic scale. (b) Longitudinal acoustic phonon dispersion of liquid iron at pressures from 16.0 to 44.9 GPa.

The hard sphere model (HSM) [32] has often been applied for the structure of a single-component liquid. For example, Ikuta *et al.* [4] determined the density of liquid aluminum up to 6.9 GPa on the basis of fitting the HSM to experimentally obtained structure factor $S(Q)$. The HSM, however, does not match the $S(Q)$ of liquid iron observed in this study at relatively large Q (Fig. S2, [10]), indicating that the structure of liquid iron at high pressure is more complex than the HSM. Similar discrepancies between observed $S(Q)$ for liquid metals and the HSM have been reported [4,33]. The densities of liquid iron obtained on the basis of the HSM are smaller than those determined by the

present analyses by ~ 3 atoms/nm³ (~ 3 –3.5%) for all of runs No. 1–11.

The sound velocity V_P of liquid iron was determined from IXS spectra collected at BL43LXU, SPring-8 [34,35] (Table I, see Supplemental Material [10], Sec. III). The molten state of a sample was confirmed by the absence of XRD peaks from solid iron, before and after the IXS measurements. The IXS spectra included three peaks in the present scanned energy range [Fig. 3(a)]; Stokes and anti-Stokes components of the longitudinal acoustic phonon mode from the sample, and a quasielastic contribution near zero energy transfer. We determined the V_P of liquid iron

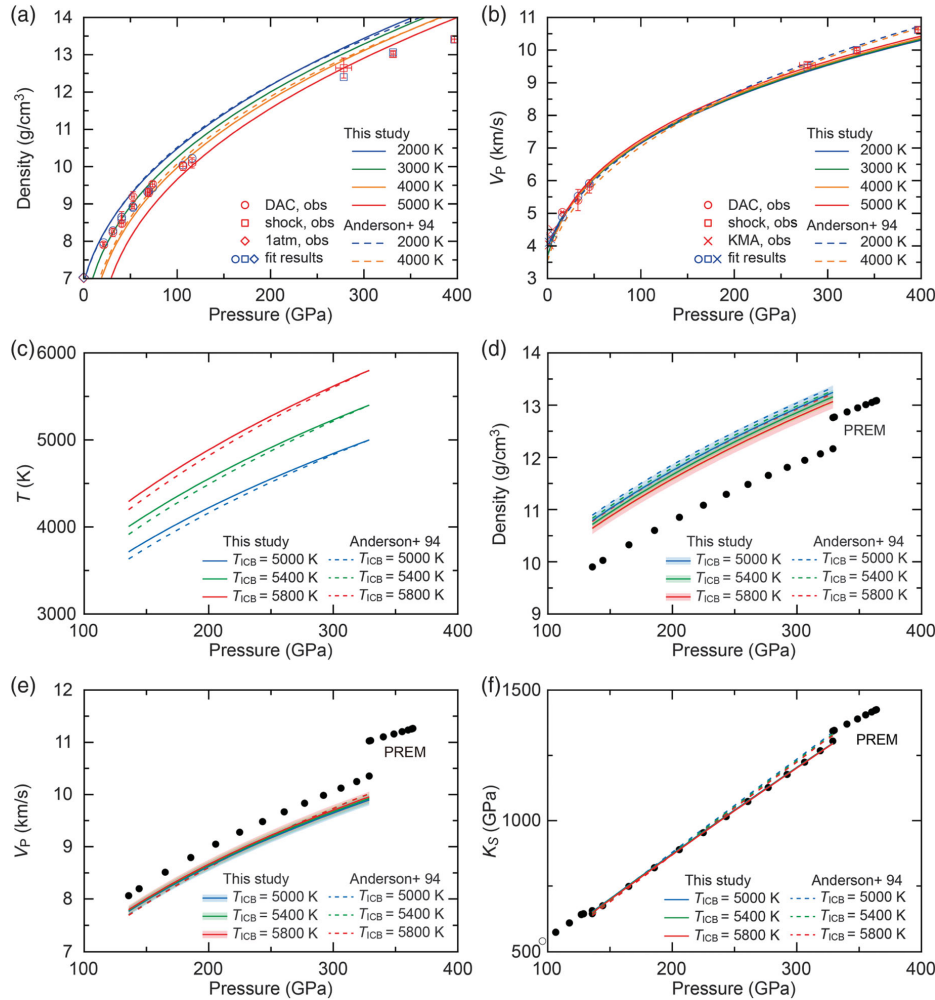


FIG. 4. Density (ρ), P -wave velocity (V_P), and adiabatic bulk modulus (K_S) of liquid iron. (a),(b) Isothermal $P-\rho$ and $P-V_P$ relations calculated from our EOS for 2000 (blue), 3000 (green), 4000 (yellow), and 5000 K (red) (Table S II [10]). Dashed lines, 2000 (red) and 4000 K (yellow), are from shock-compression study [8]. Red symbols represent experimental data (circles, this study; squares, shock experiments [8]; crosses, multi-anvil (KMA) experiments [5]; diamonds, 1 bar data at 1811 K [39]). Consistency between the red and blue (fit results) symbols indicates that our EOS well reproduces all experimental data points. (c) Calculated isentropic temperature profiles with $T_{ICB} = 5800$ K (red), 5400 K (green), and 5000 K (blue) (Table S III [10]) (see Supplemental Material [10], Sec. IV). Dashed lines are those proposed by a previous study with a different Grüneisen parameter [8]. (d),(e),(f) Comparison of seismic observations (black circles, PREM [40]) with the ρ , V_P , and K_S of liquid Fe under core pressures along the isentropic temperature profiles in (c). Uncertainties in the present estimates of ρ and V_P are $\sim 1\%$ (see the uncertainty band around each solid curve and Supplemental Material [10], Sec. IV for details). Dashed lines represent those proposed on the basis of earlier shock-wave data [8].

between 16 and 45 GPa from dispersion relations [Fig. 3(b)]. Note that the V_P of liquid iron is not sensitive to temperature [36–38]. While the structure of liquidus crystals of iron changes from face-centered-cubic (fcc) to hcp at ~ 100 GPa, it does not likely affect the $P - V_P$ relation for liquid since both are close-packed structures and such an effect is not found in the present $P - \rho$ data [Fig. 4(a)].

Now we have both $P - T - \rho$ and $P - T - V_P$ data for liquid iron from the present study, in addition to the $P - \rho - V_P - \gamma$ relation from previous shock compression experiments [8]. From these data, we obtain the $P - T - \rho - V_P - \gamma$ relation across Earth's entire outer core conditions, based on the Mie-Grüneisen EOS (see Supplemental Material [10], Sec. IV) [Figs. 4(a) and 4(b)]. We do not employ the ρ at 1 bar [39] nor the V_P determined below 5.8 GPa [5], but, even so, our EOS reproduces these data well, suggesting that a possible structural change in liquid iron below 6 GPa [6] has only a small impact on ρ and V_P .

In order to compare liquid iron properties with seismological observations [40], we calculated the isentropic T profiles using γ determined in this study (see Supplemental Material [10], Sec. IV), considering three different model temperatures at the liquid or solid core boundary (inner core boundary, ICB) ($T_{\text{ICB}} = 5000, 5400, \text{ and } 5800$ K) [3] [Fig. 4(c)]. Compared to the ρ , V_P , and adiabatic bulk modulus (K_S) of liquid iron calculated along the isentrope with $T_{\text{ICB}} = 5400$ K, Earth's liquid outer core exhibits low ρ by 0.99–0.81 g/cm³ (7.5%–7.6%) [Fig. 4(d)] and high V_P by 0.43–0.29 km/s (4.3%–3.7%) [Fig. 4(e)]. Such ρ deficit is about 1% smaller than the previous estimates of 8.4%–8.6% [8] that was based on the EOS determined by a combination of the shock-wave data [7], including their uncertain T estimates and the 1-bar data. In contrast, the observed K_S of the outer core is almost identical to that of liquid iron [Fig. 4(f)]. Note that the K_S of liquid iron is not sensitive to temperature.

Seismology gives the density difference between the liquid and solid core at the ICB; $\Delta\rho_{\text{ICB}} = 0.55\text{--}0.82$ g/cm³ [40–42]. Our results show that liquid iron is less dense than hexagonal-close-packed (hcp) iron [43] by $\Delta\rho_{\text{melting}} = 0.32$ g/cm³ at 330 GPa and its melting point of 6230 K [44]. This is larger than the previous estimates of 0.12–0.22 g/cm³ [45,46] and approximately half of the observed $\Delta\rho_{\text{ICB}}$. Therefore, the remaining 0.23–0.50 g/cm³ (corresponding to 1.9%–4.1% of the liquid core density at the ICB) should be attributed to a compositional difference between the outer and inner core ($\Delta\rho_{\text{comp}}$).

Since the solubility of oxygen (O) in solid iron is negligible [47,48], oxygen has been widely considered as a main light element in the Earth's core, in order to account for $\Delta\rho_{\text{comp}}$ [47]. Our revised density EOS of liquid iron indicates a smaller $\Delta\rho_{\text{comp}}$ that can be explained with only 1.6–3.8 wt % O in the outer core and none in the inner core. This gives the upper bound for oxygen concentration in the liquid core. However, 1.6–3.8 wt % O is not high

enough to explain the deficit of the outer core with respect to liquid pure iron [49], suggesting that oxygen is not a predominant light element in the core. While the light elements in the core have not yet been identified [3], this study revealed that the ρ deficit is constant at 7.5%–7.6% and the V_P excess is also almost constant at 4.3%–3.7% over the entire outer core [40], which strongly constrains its possible compositional range.

The EOS is a fundamental macroscopic characteristic of a material. Our new analytical procedure to derive liquid density from diffuse x-ray scattering signals can be applied to any amorphous materials and may be used to explore the equations of state of other liquids. In addition, this work demonstrates that a combination of high-pressure density and velocity data enables a precise determination of the EOS. These data can now be obtained not only for solids but for liquids via XRD and IXS measurements even at extreme high P – T conditions by using LH-DAC techniques. For further understanding the nature of amorphous materials under compression, future technical developments to use higher energy x-ray are necessary to collect diffuse signals in a wider Q range.

The authors thank H. Genda, G. Helffrich, H. Ichikawa, D. Antonangeli, G. Fiquet, F. Guyot, K. Umamoto, K. Ueki, R. Nomura, T. Kuwatani, H. Nagao, S. Ito, T. Matsumura, Y. Ando, K. Nagata, and A. Sakuraba for valuable discussions. We are grateful to H. Uchiyama for his technical support. We also thank G. Garbarino for providing the Ce-based glass data. XRD and IXS measurements were performed at BL10XU (Proposals No. 2013A0087, No. 2013B0087, No. 2014A1127, No. 2014A0080, No. 2014B0080, No. 2015A0080, No. 2015B0080, No. 2016A0080, No. 2016B0080, No. 2017A0072, No. 2017B0072, and No. 2018A0072) and at BL43LXU (Proposals No. 20160098, No. 20170056, and No. 20180008), SPring-8. This work was supported by the JSPS KAKENHI Grants No. 26800274 (Y. K.), 17K14418 (Y. N.), 24000005 and 16H06285 (K. H.), and by a CNRS exchange program (Y. K.).

*To whom correspondence should be addressed.
kuwayama@eps.s.u-tokyo.ac.jp

†To whom correspondence should be addressed.
yoichi@kumamoto-u.ac.jp

‡To whom correspondence should be addressed.
kei@elsi.jp

- [1] G. Helffrich, *Prog. Earth Planet. Sci.* **4**, 24 (2017).
- [2] A. Genova, S. Goossens, E. Mazarico, F. G. Lemoine, G. A. Neumann, W. Kuang, T. J. Sabaka, S. A. Hauck, D. E. Smith, S. C. Solomon, and M. T. Zuber, *Geophys. Res. Lett.* **46**, 3625 (2019).
- [3] K. Hirose, S. Labrosse, and J. Hernlund, *Annu. Rev. Earth Planet Sci.* **41**, 657 (2013).

- [4] D. Ikuta, Y. Kono, and G. Shen, *J. Appl. Phys.* **120**, 135901 (2016).
- [5] K. Nishida, A. Suzuki, H. Terasaki, Y. Shibazaki, Y. Higo, S. Kuwabara, Y. Shimoyama, M. Sakurai, M. Ushioda, E. Takahashi, T. Kikegawa, D. Wakabayashi, and N. Funamori, *Phys. Earth Planet. Inter.* **257**, 230 (2016).
- [6] C. Sanloup, F. Guyot, P. Gillet, G. Fiquet, R. J. Hemley, M. Mezouar, and I. Martinez, *Europhys. Lett.* **52**, 151 (2000).
- [7] J. M. Brown and G. McQueen, *J. Geophys. Res.* **91**, 7485 (1986).
- [8] W. W. Anderson and T. J. Ahrens, *J. Geophys. Res.* **99**, 4273 (1994).
- [9] Y. Ohishi, N. Hirao, N. Sata, K. Hirose, and M. Takata, *High Press. Res.* **28**, 163 (2008).
- [10] See Supplemental Material at <http://link.aps.org/supplemental/10.1103/PhysRevLett.124.165701> for additional information, which includes Refs. [11–24].
- [11] K. Ohta, Y. Kuwayama, K. Hirose, K. Shimizu, and Y. Ohishi, *Nature (London)* **534**, 95 (2016).
- [12] Y. Seto, D. Nishio-Hamane, T. Nagai, and N. Sata, *Rev. High Pres. Sci. Tech.* **20**, 269 (2010).
- [13] N. Tsujino, Y. Nishihara, Y. Nakajima, E. Takahashi, K.-i Funakoshi, and Y. Higo, *Earth Planet. Sci. Lett.* **375**, 244 (2013).
- [14] A. Dewaele, A. B. Belonoshko, G. Garbarino, F. Occelli, P. Bouvier, M. Hanfland, and M. Mezouar, *Phys. Rev. B* **85**, 214105 (2012).
- [15] *International Tables for Crystallography*, 3rd ed., edited by E. Prince (IUC, 2004).
- [16] R. Kaplow, S. L. Strong, and B. L. Averbach, *Phys. Rev.* **138**, A1336 (1965).
- [17] G. Morard, G. Garbarino, D. Antonangeli, D. Andrault, N. Guignot, J. Siebert, M. Roberge, E. Boulard, A. Lincot, A. Denoeud, and S. Petitgirard, *High Press. Res.* **34**, 9 (2014).
- [18] B. Zhang, R. J. Wang, D. Q. Zhao, M. X. Pan, and W. H. Wang, *Phys. Rev. B* **70**, 224208 (2004).
- [19] A. Q. R. Baron, *SPRING-8 Inf. Newsl.* **15**, 14 (2010).
- [20] T. Scopigno, G. Ruocco, and F. Sette, *Rev. Mod. Phys.* **77**, 881 (2005).
- [21] S. I. Kawaguchi, Y. Nakajima, K. Hirose, T. Komabayashi, H. Ozawa, S. Tateno, Y. Kuwayama, S. Tsutsui, and A. Q. R. Baron, *J. Geophys. Res.* **122**, 3624 (2017).
- [22] H. Ichikawa, T. Tsuchiya, and Y. Tange, *J. Geophys. Res.* **119**, 240 (2014).
- [23] T. Matsumura, Y. Kuwayama, K. Nagata, Y. Ando, T. Kuwatani, K. Ueki, S. Ito, and H. Nagao (to be published).
- [24] F. Wagle and G. Steinle Neumann, *J. Geophys. Res.* **124**, 3350 (2019).
- [25] J. H. Eggert, G. Weck, P. Loubeyre, and M. Mezouar, *Phys. Rev. B* **65**, 174105 (2002).
- [26] C. Sanloup, J. W. E. Drewitt, Z. Konôpková, P. Dalladay-Simpson, D. M. Morton, N. Rai, W. Van Westrenen, and W. Morgenroth, *Nature (London)* **503**, 104 (2013).
- [27] G. Morard, J. Siebert, D. Andrault, N. Guignot, G. Garbarino, F. Guyot, and D. Antonangeli, *Earth Planet. Sci. Lett.* **373**, 169 (2013).
- [28] J. Krogh-Moe, *Acta Crystallogr.* **9**, 951 (1956).
- [29] N. Norman, *Acta Crystallogr.* **10**, 370 (1957).
- [30] T. Sato, N. Funamori, and T. Kikegawa, *Rev. Sci. Instrum.* **81**, 043906 (2010).
- [31] K. Furukawa, *Rep. Prog. Phys.* **25**, 395 (1962).
- [32] N. W. Ashcroft and J. Lekner, *Phys. Rev.* **145**, 83 (1966).
- [33] G. Shen, M. L. Rivers, S. R. Sutton, N. Sata, V. B. Prakapenka, J. Oxley, and K. S. Suslick, *Phys. Earth Planet. Inter.* **143–144**, 481 (2004).
- [34] A. Q. R. Baron, in *Synchrotron Light Sources, and Free-Electron Lasers: Accelerator Physics, Instrumentation, and Science Applications*, edited by E. J. Jaeschke, S. Khan, J. R. Schneider, and J. B. Hastings (Springer, New York, 2016), pp. 1643–1757.
- [35] A. Q. R. Baron, D. Ishikawa, H. Fukui, and Y. Nakajima, *AIP Conf. Proc.* **2054**, 020002 (2019).
- [36] L. Vočadlo, D. Alfè, M. J. Gillan, and G. D. Price, *Phys. Earth Planet. Inter.* **140**, 101 (2003).
- [37] Y. Nakajima, S. Imada, K. Hirose, T. Komabayashi, H. Ozawa, S. Tateno, S. Tsutsui, Y. Kuwayama, and A. Q. R. Baron, *Nat. Commun.* **6**, 8942 (2015).
- [38] K. Umemoto and K. Hirose, *Geophys. Res. Lett.* **42**, 7513 (2015).
- [39] M. J. Assael, K. Kakosimos, R. M. Banish, J. Brillo, I. Egry, R. Brooks, P. N. Quested, K. C. Mills, A. Nagashima, Y. Sato, and W. A. Wakeham, *J. Phys. Chem. Ref. Data* **35**, 285 (2006).
- [40] A. M. Dziewonski and D. L. Anderson, *Phys. Earth Planet. Inter.* **25**, 297 (1981).
- [41] T. G. Masters and P. M. Shearer, *J. Geophys. Res.* **95**, 21691 (1990).
- [42] G. Masters and D. Gubbins, *Phys. Earth Planet. Inter.* **140**, 159 (2003).
- [43] A. Dewaele, P. Loubeyre, F. Occelli, M. Mezouar, P. I. Dorogokupets, and M. Torrent, *Phys. Rev. Lett.* **97**, 215504 (2006).
- [44] S. Anzellini, A. Dewaele, M. Mezouar, P. Loubeyre, and G. Morard, *Science* **340**, 464 (2013).
- [45] O. L. Anderson, in *Earth's Core: Dynamics, Structure, Rotation*, edited by V. Dehant, K. C. Creager, S. Karato, and S. Zatman (AGU, Washington, DC, 2003), pp. 83–103.
- [46] J. P. Poirier, *Geophys. J. R. Astron. Soc.* **85**, 315 (1986).
- [47] D. Alfè, M. J. Gillan, and G. D. Price, *Earth Planet. Sci. Lett.* **195**, 91 (2002).
- [48] H. Ozawa, K. Hirose, S. Tateno, N. Sata, and Y. Ohishi, *Phys. Earth Planet. Inter.* **179**, 157 (2010).
- [49] J. Badro, A. S. Cote, and J. P. Brodholt, *Proc. Natl. Acad. Sci. U.S.A.* **111**, 7542 (2014).